Physics Letters B 775 (2017) 271–276

Contents lists available at ScienceDirect

Physics Letters B

www.elsevier.com/locate/physletb

Nucleon correlations and the structure of $^{71}_{30}Zn_{41}$

S. Bottoni [a,*,1], S. Zhu [a,*], R.V.F. Janssens [a,2], M.P. Carpenter [a], Y. Tsunoda [b], T. Otsuka [b,c,d,e,f], A.O. Macchiavelli [g], D. Cline [h], C.Y. Wu [i], A.D. Ayangeakaa [a,3], B. Bucher [i,4], M.Q. Buckner [i], C.M. Campbell [g], C.J. Chiara [a,j,5], H.L. Crawford [g], M. Cromaz [g], H.M. David [a,6], P. Fallon [g], A. Gade [e,k], J.P. Greene [a], J. Harker [a,j], A.B. Hayes [l], C.R. Hoffman [a], B.P. Kay [a], A. Korichi [m], T. Lauritsen [a], J. Sethi [a,j], D. Seweryniak [a], W.B. Walters [j], D. Weisshaar [e], A. Wiens [g]

[a] Physics Division, Argonne National Laboratory, Argonne, IL 60439, USA
[b] Center for Nuclear Study, University of Tokyo, Hongo, Bunkyo-ku, Tokyo 113-0033, Japan
[c] Department of Physics, University of Tokyo, Hongo, Bunkyo-ku, Tokyo 113-0033, Japan
[d] RIKEN Nishina Center, 2-1 Hirosawa, Wako, Saitama 351-0198, Japan
[e] National Superconducting Cyclotron Laboratory, Michigan State University, East Lansing, MI 48824, USA
[f] Instituut voor Kern- en Stralingsfysica, KU Leuven, B-3001 Leuven, Belgium
[g] Nuclear Science Division, Lawrence Berkeley National Laboratory, Berkeley, CA 94720, USA
[h] Department of Physics, University of Rochester, Rochester, NY 14627, USA
[i] Lawrence Livermore National Laboratory, Livermore, CA 94551, USA
[j] Department of Chemistry and Biochemistry, University of Maryland, College Park, MD 20742, USA
[k] Department of Physics and Astronomy, Michigan State University, East Lansing, MI 48824, USA
[l] Institute of Optics, University of Rochester, Rochester, NY 14627, USA
[m] CSNSM-IN2P3, F-91405 Orsay Campus, France

ARTICLE INFO

Article history:
Received 30 August 2017
Received in revised form 3 October 2017
Accepted 1 November 2017
Available online 6 November 2017
Editor: D.F. Geesaman

ABSTRACT

The structure of ^{71}Zn was investigated by one-neutron transfer and heavy-ion induced complex (deep-inelastic) reactions using the GRETINA-CHICO2 and the Gammasphere setups, respectively. The observed inversion between the $9/2^+$ and $1/2^-$ states is explained in terms of the role of neutron pairing correlations. Non-collective sequences of levels were delineated above the $9/2^+$ isomeric state. These are interpreted as being associated with a modest oblate deformation in the framework of Monte-Carlo shell-model calculations carried out with the A3DA-m Hamiltonian in the $pfg_{9/2}d_{5/2}$ valence space. Similarities with the structure of $^{68}_{28}Ni_{40}$ were observed and the shape-coexistence mechanism in the $N = 40$ region of neutron-rich nuclei is discussed in terms of the so-called *Type-II* shell evolution, with an emphasis on proton–neutron correlations between valence nucleons, especially those involving the shape-driving $g_{9/2}$ neutron orbital.

Shell structure is a cornerstone in the description of atomic nuclei as many-body quantum systems. Data on neutron-rich nuclei far from stability have provided conclusive evidence that shell structure evolves with neutron excess and, for example, some well-known magic numbers disappear while others appear [1,2]. The development of new experimental techniques has facilitated the discovery of unexpected structural properties in exotic nuclei which, in turn, have stimulated the introduction of new theoretical concepts [3,4].

It has been shown that effective single-particle energies are significantly modified in neutron-rich systems through the action of the monopole component of the proton–neutron tensor force [5]. Furthermore, multi-particle multi-hole excitations trigger shell evolution as a function of spin and excitation energy, a process that has been referred to as *Type-II* shell evolution [3,6], where the occupation of specific deformation-driving orbitals leads to

* Corresponding authors.
E-mail addresses: simone.bottoni@mi.infn.it (S. Bottoni), zhu@anl.gov (S. Zhu).

[1] Present address: Università degli Studi di Milano and INFN, Via Celoria 16, 20133 Milano, Italy.

[2] Present address: Dept. of Physics and Astronomy, University of North Carolina at Chapel Hill, Chapel Hill, North Carolina 27599-3255, and Triangle Universities Nuclear Laboratory, Duke University, Durham, North Carolina 27708-2308, USA.

[3] Present address: Physics Department, U.S. Naval Academy, Annapolis, MD 21402, USA.

[4] Present address: Idaho National Laboratory, Idaho Falls, ID 83415, USA.

[5] Present address: U.S. Army Research Laboratory, Adelphi, MD 20783, USA.

[6] Present address: GSI Helmholtzzentrum für Schwerionenforschung, 6429 Darmstadt, Germany.

https://doi.org/10.1016/j.physletb.2017.11.003

changes in the nuclear shape and to the possibility of shape coexistence [7].

In this context, the neutron-rich nuclei around neutron number $N = 40$ have attracted much attention since the discovery of a neutron subshell closure and of triple shape coexistence in ^{68}Ni [8–10]. However, studies in the vicinity of the latter indicate that this subshell closure is rather weak and that neighboring nuclei quickly gain deformation and collectivity, built in part on particle–hole configurations involving the intruder $\nu g_{9/2}$ neutron orbital [11–22].

With two protons and a single neutron outside "doubly-magic" ^{68}Ni, ^{71}Zn would be expected to be characterized by a $9/2^+$ ground state, as is the case for its adjacent $N = 41$ isotones ^{69}Ni and ^{73}Ge. However, the spin and parity of the ^{71}Zn ground state is $1/2^-$, while the $9/2^+$ level is located 158 keV above it and is isomeric ($T_{1/2} = 3.96$ h) [23]. At present, there is no generally accepted explanation for this apparent level inversion. A possible ground-state configuration could involve a $p_{1/2}$ neutron hole, *e.g.*, $\nu p_{1/2}^{-1} g_{9/2}^2$, where the occupation of the $g_{9/2}$ orbital by the two neutrons would be shape driving and result in the inversion. While studies of the ^{70}Zn(d, p) reaction indicate that the strength of the $\nu p_{1/2}$ single-particle state is concentrated in the ground state [24], recent data of Ref. [25] suggest coexistence of single-particle and collective excitations at low energies. On the other hand, recent collinear laser spectroscopy results on the Zn isotopic chain indicate an onset of collectivity only for $N \geq 43$ [26]. However, the available experimental information is scarce and a more detailed spectroscopic investigation of ^{71}Zn would provide an opportunity to better understand the exact nature of its excitations and the mechanism(s) responsible for its structure. In particular, no transitions feeding the $9/2^+$ isomeric state have been reported thus far [23]. In this letter, the level structure of ^{71}Zn is explored to fairly high spin. The data enable a focus of the discussion of level inversion on the role of neutron–neutron pairing. The impact of proton–neutron interactions on the nuclear shape is addressed as well.

Two separate experiments were carried out at the ATLAS facility at Argonne National Laboratory. In the first, the nucleus of interest was populated via the ^{70}Zn(^{48}Ca, ^{47}Ca)^{71}Zn one-neutron, direct-transfer reaction with a 170-MeV beam on a 1.6-mg/cm^2 ^{70}Zn target. The experimental setup comprised the GRETINA γ-ray tracking spectrometer [27] coupled to the CHICO2 charged-particle detector [28]. In the second experiment, ^{71}Zn was populated via deep-inelastic collisions induced by a 430-MeV ^{70}Zn beam on a ^{197}Au target sufficiently thick to stop the reaction products and the beam. The Gammasphere array [29] in stand-alone mode was used to collect events with the requirement of three or more γ rays measured in coincidence.

If present, deformed states in ^{71}Zn are likely to have short intrinsic lifetimes and deexciting transitions would be fast. Consequently, the emitted γ rays are possibly undetectable in a thick-target experiment because of Doppler broadening. The combination of GRETINA and CHICO2 allowed for the proper Doppler reconstruction of γ rays from nuclei decaying in flight. In addition, the direct-transfer reaction provided clearer assignments of observed γ rays to ^{71}Zn, especially for transitions associated with the isomeric state. The GRETINA array consisted of 28 highly-segmented high-purity germanium crystals, grouped into seven clusters, with four crystals each. The decomposition of the digitized traces enabled the determination of the interaction points of each γ ray within the crystals, and these were used to reconstruct the photon trajectories and energies by means of a tracking algorithm based on Compton scattering [27,30]. The CHICO2 heavy-ion detector consisted of two symmetrical hemispheres around the target, holding ten position-sensitive parallel-plate avalanche counters

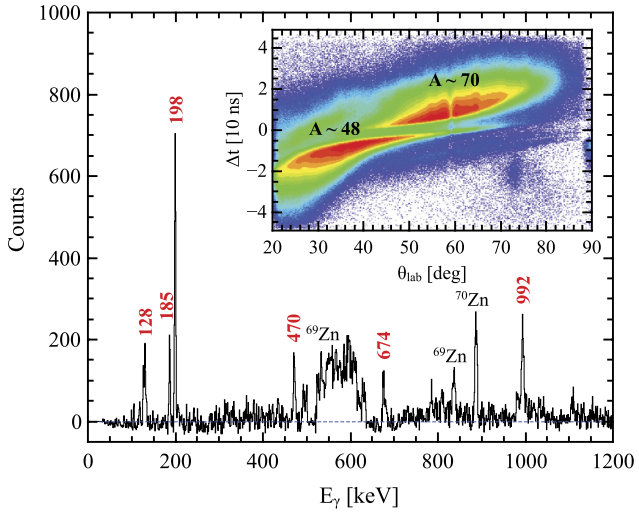

Fig. 1. Particle-gated γ-ray spectrum measured with GRETINA displaying transitions from target-like products in coincidence with the 2013.5-keV γ ray in ^{47}Ca. The majority of the peaks were assigned to ^{71}Zn (red labels), but those from other products are labeled accordingly. The broad structure between 500 and 650 keV is due mainly to transitions in ^{47}Ca for which the Doppler correction is inappropriate. Inset: particle spectrum from CHICO2 presenting the time-of-flight difference between the reaction partners as a function of the scattering angle. The separation between target- and projectile-like reaction products is illustrated. (For interpretation of the references to color in this figure legend, the reader is referred to the web version of this article.)

each [28]. It covered a total solid angle of 69% of 4π, with the anode and cathode segmentation achieving angular resolutions of 1.6° in the polar angle θ and 2.5° in the azimuthal one ϕ, respectively.

The inset of Fig. 1 presents the particle spectrum measured in the experiment. Although CHICO2 does not provide unit mass and Z resolution, its 1.2-ns time resolution (FWHM) allowed to separate and identify the projectile-like and target-like nuclei with $A \sim 48$ and $A \sim 70$, respectively, by correlating the time-of-flight difference between the reaction partners with the scattering angles. This also enabled the event-by-event reconstruction of the reaction kinematics, using an average Q-value. This capability, along with the 2-mm position resolution (σ) of GRETINA, resulted in a precise Doppler correction of the γ-ray spectra measured in coincidence with the reaction products. It is interesting to note that the direct nature of the reaction can be inferred from the particle spectrum in the inset of Fig. 1, as the angular distributions of the reaction products are peaked in specific angular regions.

The level and γ-decay schemes of ^{71}Zn were established by means of γ–γ coincidence relationships, using the proper Doppler correction according to the recoil-gate used. The low-lying γ rays in ^{71}Zn were identified by cross-correlating ^{47}Ca and ^{71}Zn, gating on the 2013.5-keV ground-state transition in ^{47}Ca; see Fig. 1. The high transition energy of the latter ensures that the residual internal excitation in ^{71}Zn is rather low, taking the reaction Q-value of -4.1 MeV into account. Furthermore, the binary character of the reaction guarantees that ^{71}Zn is the strongest reaction partner of ^{47}Ca, with smaller contributions from ^{70}Zn and ^{69}Zn corresponding to one- and two-neutron evaporation, respectively ($S_n = 5.8$ MeV and $S_{2n} = 15.1$ MeV) [31]. The observed γ rays and γ–γ coincidence relationships in the target-like channel were used to establish the level scheme of ^{71}Zn.

The ^{71}Zn structure was investigated further in the second experiment with Gammasphere. The γ rays emitted at rest were studied using triple γ-ray coincidence relationships based on transitions assigned to ^{71}Zn in the analysis of the above data. The level scheme was extended to higher excitation energies as a re-

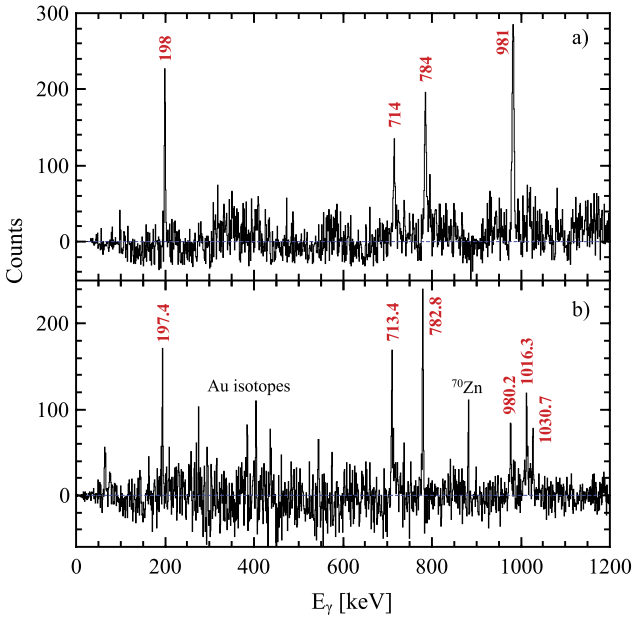

Fig. 2. (a) Double-coincidence spectrum measured with GRETINA. Besides a particle gate on $A \sim 70$ reaction products, a coincidence with the 1030.7-keV transition is required; (b) Sum of triple-coincidence spectra measured by Gammasphere with double-coincidence gates placed on the (197.4- and 1030.7-keV), (197.4- and 782.8-keV), (1030.7- and 782.8-keV) and (1030.7- and 713.4-keV) pairs. Energy discrepancies between the two experiments are due to uncertainties related to Doppler shift in the GRETINA data set (see text for details).

sult of the reaction mechanism employed which favors population of high-spin, yrast states. Representative spectra from the two experiments can be compared in Figs. 2(a) and (b) for data taken with GRETINA and Gammasphere, respectively. Note that the small differences between the transition energies in Figs. 2(a) and (b) are within the 1–1.5 keV uncertainties in the GRETINA spectra associated with the Doppler-shift corrections for γ rays emitted in flight.

The partial level scheme obtained in this work is presented in Fig. 3, where the more precise γ-ray energies of the Gammasphere experiment were adopted; these are also used in the discussions below. The 197- and 991-keV γ rays measured in the GRETINA experiment allowed for the first identification of two sequences built on the $9/2^+$, 3.96-h isomeric state. These sequences were extended further with the Gammasphere data up to an excitation energy of ~ 6 MeV. The γ-ray angular distributions of the 991-, 980-, and 197-keV transitions were studied as a function of the angle between the recoils detected by CHICO2 and the γ-ray direction determined from GRETINA. The measured intensities were corrected with the help of a GEANT4-simulated response of the GRETINA array for the detection of an isotropic γ ray [32]. Following this procedure, the 991- and 980-keV transitions were established to be of quadrupole and dipole character, respectively, while the 197-keV γ ray was determined to be of mixed $\lambda = 1$ and $\lambda = 2$ multipolarity. Based on the coincidence relationships, the angular distributions, and the γ-ray intensities, a detailed level scheme was obtained, comprised of distinct sets of levels built on the $1/2^-$ ground state and $9/2^+$ isomer. This complete level scheme will be presented in a forthcoming publication [33], while the focus here is on the sequences built on the long-lived $9/2^+$ state.

From the available experimental evidence as well as from results of calculations presented hereafter, the two sequences of Fig. 3 are proposed to be composed of positive-parity states linked by quadrupole in-band transitions and dipole inter-band ones. The $7/2^+$, 355.1-keV level is noteworthy as it was not observed in the ^{70}Zn(d, p) reaction [24] where the strength associated with the $\nu g_{7/2}$ single-particle state was found to be concentrated at higher excitation energy, as expected for an orbital located above the $N = 50$ shell gap. Hence, the intrinsic structure of the 355.1-keV state and of the other members of the sequence is likely more complex. Another indication about the nature of this sequence, and of the one built on the $9/2^+$ level, comes from the fact that all transitions are observed as narrow γ-ray peaks without any evidence of Doppler broadening in the deep-inelastic data where a thick target was used (see Fig. 2(b)). This argues for intrinsic state lifetimes longer than the stopping time in the target material, as would be expected when collectivity is weak or absent. The results of the present work do not provide a signature for the presence of strong prolate deformation as neither of the sequences built on the $9/2^+$ isomer (Fig. 3 and discussion above) nor the states built on the ground state (not shown) display signs of collectivity through the presence of regular level patterns or fast transitions. Hence, the inversion of the $9/2^+$ and $1/2^-$ levels cannot be attributed to the lowering in energy of the intruder $\nu g_{9/2}$ orbital due to the presence of sizable deformation.

In order to gain further insight into the nature of such inversion in ^{71}Zn, large-scale shell-model calculations were carried out using the JUN45 [34], and the jj44b [35] Hamiltonians within a valence space restricted to the $f_{5/2}pg_{9/2}$ orbitals for both protons and neutrons with a ^{56}Ni core. This approach with a limited model space is thought to be adequate for states near the groundstate. Among these two interactions, the latter one, which is fit primarily on $Z = 28$–30 and $N = 48$–50 nuclei, better reproduces the ^{71}Zn level structure at low spins, including the $1/2^-$ ground state [33]. Based on these calculations, a potential explanation for the crossing of these two states relates to the difference in pairing strength between pairs of neutrons occupying the $\nu p_{1/2}$ and the $\nu g_{9/2}$ orbitals. To explore this possibility, the BCS equations were solved in the $\nu pf_{5/2}g_{9/2}$ valence space to calculate neutron quasi-particle energies, using single-particle values provided by the jj44b effective interaction (0.0, 0.37, 1.39, and 3.76 MeV for the $p_{3/2}$, $f_{5/2}$, $p_{1/2}$, and $g_{9/2}$ orbitals, respectively). The neutron pairing gap, Δ_n, was investigated as a function of the neutron number N. The pairing strength was set to $G_n^{pairing} = 23.5$ MeV so that the Δ_n value for ^{71}Zn matched that derived from the so-called four-point formula [31,36]. The Δ_n results for the Zn isotopic chain are given in Fig. 4(a), while the computed $\nu p_{1/2}$ and $\nu g_{9/2}$ quasi-particle energies (ϵ_ν) are displayed in Fig. 4(b). A $p_{1/2}$–$g_{9/2}$ crossing is seen to occur at ^{71}Zn, where the two orbitals are within 180 keV of each other. Hence, it is likely, or at least possible, that the inversion occurs as a result of the neutron pairing interaction which leads to nearly-degenerate $\nu p_{1/2}$ and $\nu g_{9/2}$ quasiparticle states near the Fermi surface. As the inversion does not occur in the ^{69}Ni and ^{73}Ge isotones, the role of protons cannot be ignored, a point discussed further below.

For understanding the higher excitation states observed above the $9/2^+$ state, a large-scale Monte Carlo shell-model calculations (MCSM) was carried out with the A3DA-m Hamiltonian [37], which uses the larger $pfg_{9/2}d_{5/2}$ space with the two-body matrix elements adopted from the GXPF1A [38] and JUN45 effective interactions, in the more restricted spaces where they apply, and from the G-matrix effective interaction with minor phenomenological modifications for matrix elements involving states in the extended space. Note that the JUN45 Hamiltonian has, in general, provided a satisfactory description of neutron-rich nuclei around $N = 40$, such as ^{65,67}Cu [39] or ^{67}Ni [22]. Fig. 3 compares the sequences observed above the $9/2^+$ state with the results of MCSM calculations. The A3DA-m Hamiltonian handles excitations involving the $f_{7/2}$, $g_{9/2}$ and $d_{5/2}$ orbitals and predicts nearly degenerate $9/2^+$ and $1/2^-$ levels, although it does not reproduce the inversion. How-

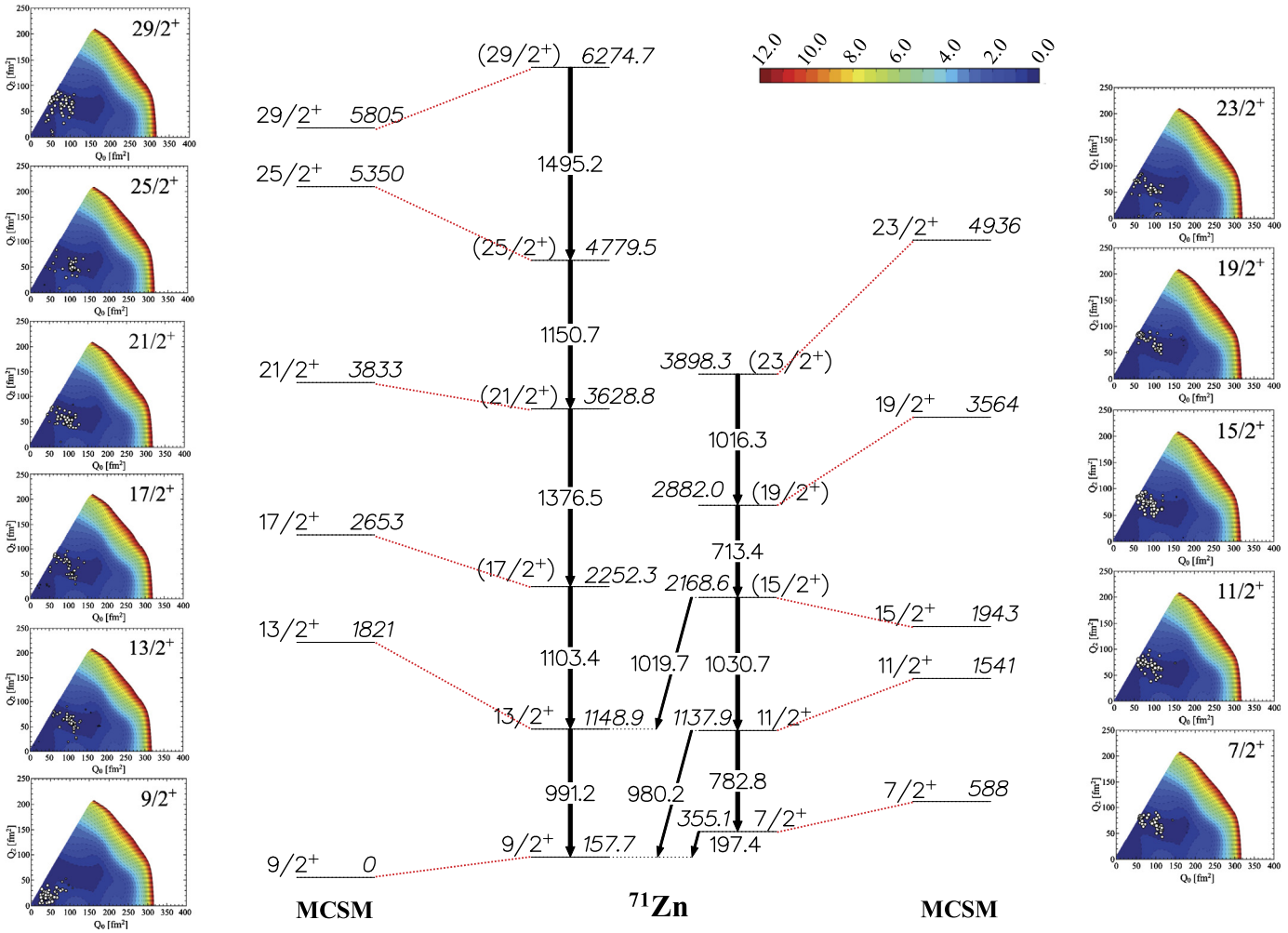

Fig. 3. Experimental partial γ-decay scheme of ^{71}Zn, showing two sequences built on the $9/2^+$ isomeric state, compared with the results of MCSM calculations performed in the $pfg_{9/2}d_{5/2}$ valence space, using the A3DA-m Hamiltonian. The figure also provides Potential Energy Surface calculations for each state, indicating that their wave functions are concentrated in the spherical ($9/2^+$ state) and in the oblate-deformed regions (other states). (For interpretation of the colors in this figure, the reader is referred to the web version of this article.)

ever, the two states are computed to lie within 350 keV of each other, i.e., within the typical uncertainty associated with this type of calculations. As illustrated in Fig. 3, the MCSM results reproduce the two sets of levels above the $9/2^+$ state, including the relative ordering between them. This figure also provides the so-called T-plots made on the Potential Energy Surfaces associated with the various excitations [3,6]. These indicate that the wave function for the $9/2^+$ state is concentrated at sphericity, but that all the other levels, up to the highest one observed, have their wave functions located in a weak minimum at or near the oblate axis, corresponding to an average deformation parameter $\beta_2 = 0.2$.

Thus, the results of these calculations are in line with the conclusions drawn above from the data. They also agree with the conclusions drawn for the $9/2^+$ level from laser spectroscopy [26].

The calculated structural change near the bandhead can be understood in terms of the neutron occupation of various orbitals. This is illustrated in Fig. 5 where the MCSM occupancies are displayed as a function of spin. The transition from a spherical to an oblate shape of small deformation results from additional excitations of neutrons into the $g_{9/2}$ orbital accompanied by a depletion of the $p_{1/2}$ and $f_{5/2}$ states. The microscopic origin of these changes in occupancy is linked to the migration of the effective single-particle energies (ESPEs) as a result of particle–hole (p–h) excitations; i.e., the so-called *Type-II* shell evolution mechanism [3]. The ESPEs for ^{71}Zn are calculated with respect to ^{70}Zn following the standard filling scheme. Thus, ^{71}Zn is viewed as a ^{68}Ni $\otimes$ $(\pi p_{3/2})^2$ ^{70}Zn ground state with an additional neutron above the $N = 40$ subshell. As the occupancies show, the core excitation reproducing the data requires the promotion of additional neutrons into the shape-driving $g_{9/2}$ orbital. This increased occupation results in a reduced splitting between the proton $f_{5/2}$ and $f_{7/2}$ spin–orbit partners as a consequence of the $\pi f_{5/2}$–$\nu g_{9/2}$ attraction and $\pi f_{7/2}$–$\nu g_{9/2}$ repulsion due to the monopole component of the tensor force, herewith enhancing the probability of p–h excitations. Nevertheless, the data indicate that this force is not sufficient to drive ^{71}Zn towards a prolate shape. This can be understood by comparing the structure of the two sequences discussed here with those associated with the 0_1^+, 0_2^+, and 0_3^+ spherical, oblate- and prolate-deformed states in ^{68}Ni.

Fig. 6 compares the MCSM calculations of proton and neutron occupancies in ^{71}Zn and ^{68}Ni for the orbitals active in the model space. For ^{71}Zn, these occupancies relate to the $9/2^+$ and $7/2^+$ levels while they are for the 0_1^+, 0_2^+ and 0_3^+ states in ^{68}Ni. It is seen that the neutron occupancies for the $9/2^+$ spherical and $7/2^+$ oblate-deformed levels are similar to those for the ^{68}Ni 0_1^+ and 0_2^+ states. The somewhat larger $\nu g_{9/2}$ occupancy that applies to ^{71}Zn is caused by the presence of the odd neutron above the $N = 40$ subshell gap. The situation for protons is similar, however, with an

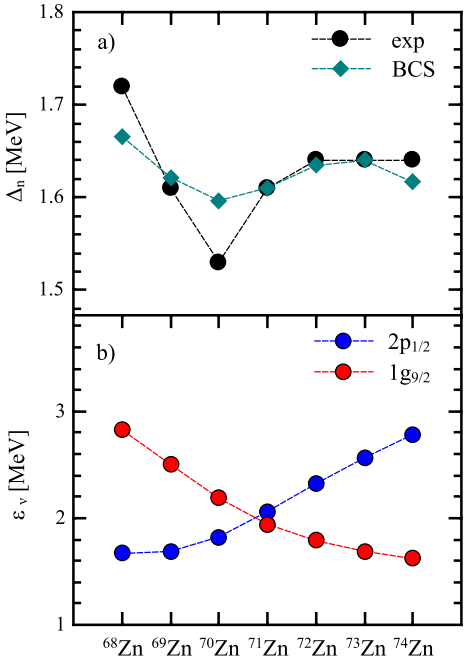

Fig. 4. (a) Pairing gap as a function of N calculated with a pairing strength $G_n^{pairing} = 23.5$ MeV (green diamonds), compared with experimental values extracted with the four-point formula (black dots) [31,36]. (b) Quasi-particle energies of the $\nu p_{1/2}$ and $\nu g_{9/2}$ orbitals (blue and red dots, respectively), showing the level crossing in ^{71}Zn (see text for details). (For interpretation of the references to color in this figure legend, the reader is referred to the web version of this article.)

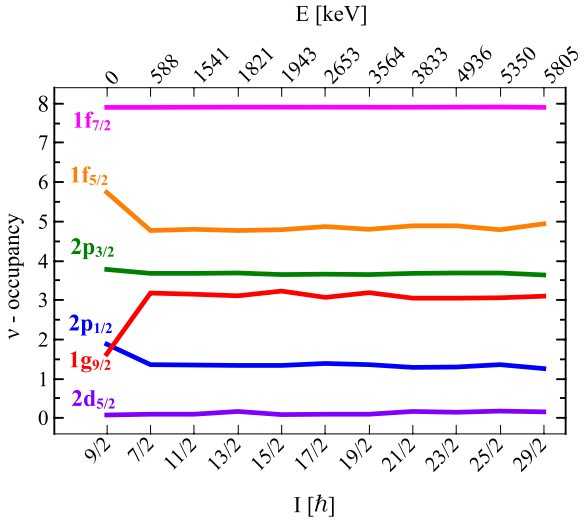

Fig. 5. MCSM occupancies of the neutron orbitals included in the valence space as a function of angular momentum, showing the difference between the $9/2^+$ level occupancy and that of the other positive-parity members of the observed sequences.

increased occupancy of the $\pi p_{3/2}$ orbital reflecting the presence of two additional protons. In ^{68}Ni, the transition to the configuration associated with the 0_3^+ prolate state involves the promotion of additional neutrons into the $\nu g_{9/2}$ orbital which results in more p–h excitations involving the $\pi f_{5/2}$–$\pi f_{7/2}$ states [6]. This process is hindered in ^{71}Zn, as the presence of two $p_{3/2}$ protons blocks some of the aforementioned $\pi(p$–$h)$ excitations.

Finally, the shell-evolution framework discussed above can also be invoked to account for the unique occurrence of the $1/2^-$ ground state in ^{71}Zn (with respect to the $N = 41$ isotones). While the $N = 40$ subshell gap is substantial in the Ni isotopes and prevents two neutrons from occupying the $g_{9/2}$ orbital, it is reduced by two additional protons across the $Z = 28$ gap in the Zn isotopes as the result of the enhanced $\pi f_{5/2}$–$\nu g_{9/2}$ attraction. Its size is, however, not lowered enough to enable the additional $\nu g_{9/2}$ occupation required to drive ^{71}Zn to a prolate $9/2^+$ ground state. The addition of two more protons in ^{73}Ge reduces the $N = 40$ gap further, herewith facilitating the population of the shape-driving $\nu g_{9/2}$ orbital. This description is consistent with the collective band structure built on both the negative- and positive-parity states reported recently in ^{73}Ge [40] as well as with the deformation derived from Coulomb excitation for ^{72}Ge [41].

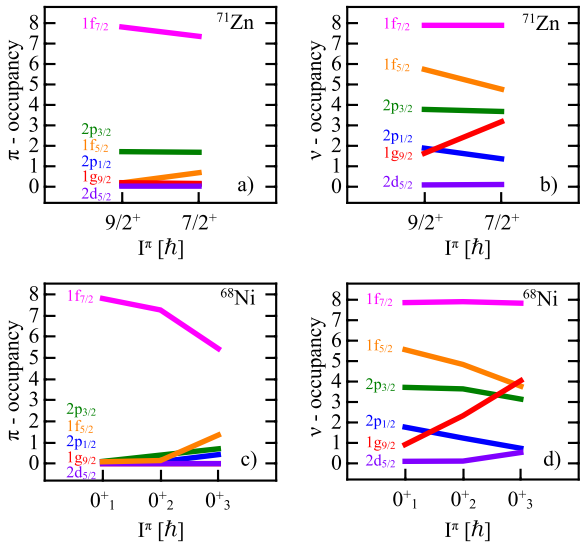

Fig. 6. MCSM calculations of proton and neutron occupancies in ^{71}Zn for orbitals included in the valence space (a–b). The spherical $9/2^+$ state and the oblate-deformed $7/2^+$ state are shown and compared with similar calculations for proton and neutron occupancies in ^{68}Ni (c–d adapted from [6]) for the 0_1^+, 0_2^+, and 0_3^+ spherical, oblate-deformed, and prolate-deformed states, respectively. (For interpretation of the colors in this figure, the reader is referred to the web version of this article.)

In conclusion, the structure of ^{71}Zn was investigated in two separate experiments, where the nucleus of interest was populated via one-nucleon transfer and deep-inelastic reactions. The level scheme was extended above the $9/2^+$ isomeric state up to $\sim$ 6 MeV in excitation energy and $(29/2)\ \hbar$ in spin through the observation of two irregularly-spaced sequences built on it. The strength of neutron–neutron pairing was found to play a role in the inversion of the $1/2^-$ and $9/2^+$ states. In addition, the transition from the spherical shape characterizing the $9/2^+$ isomer to the oblate-deformed one associated with the levels above was understood in the framework of *Type-II* shell evolution. MCSM calculations with the A3DA-m Hamiltonian showed modifications of the proton ESPEs caused by variations in the strength of the proton–neutron interactions as a function of the valence nucleons involved. The results presented in this work provide an important step towards understanding shell evolution in neutron-rich nuclei around $N = 40$ and highlight the role played by the different components of the nucleon–nucleon interactions above ^{68}Ni.

Acknowledgements

This work is supported by the U.S. Department of Energy, Office of Nuclear Physics, under Contract Nos. DE-AC02-06CH11357 (ANL), DE-AC02-05CH11231 (LBNL, GRETINA), DE-AC52-07NA27344 (LLNL), and Grants No. DE-FG02-94ER40834 (Maryland), DE-FG02-08ER41556 (MSU) and NSF under grant No. PHY-1102511 (MSU). The MCSM calculations were performed on the K computers at RIKEN AICS (hp150224, hp160211, hp170230). This work was supported in part by the HPCI strategic program (The Origin of Mat-

ter and the Universe) and “Priority Issue on post-K Computer” (Elucidation of the Fundamental Laws and Evolution of the Universe) from MEXT and JICFuS. This research used resources of ANL’s ATLAS facility, which is a DOE Office of Science User Facility. GRETINA was funded by the U.S. DOE Office of Science, Office of Nuclear Physics by the ANL and LBNL contract numbers above.

References

[1] O. Sorlin, M.-G. Porquet, Prog. Part. Nucl. Phys. 61 (2008) 602.
[2] R.V.F. Janssens, Nature 459 (2009) 1069.
[3] T. Otsuka, Y. Tsunoda, J. Phys. G, Nucl. Part. Phys. 43 (2016) 024009.
[4] A. Poves, J. Phys. G, Nucl. Part. Phys. 43 (2016) 020401.
[5] T. Otsuka, et al., Phys. Rev. Lett. 95 (2005) 232502.
[6] Y. Tsunoda, et al., Phys. Rev. C 89 (2014) 031301(R).
[7] A. Gade, S.N. Liddick, J. Phys. G, Nucl. Part. Phys. 43 (2016) 024001.
[8] R. Broda, et al., Phys. Rev. Lett. 74 (1995) 868;
R. Broda, et al., Phys. Rev. C 86 (2012) 064312.
[9] F. Recchia, et al., Phys. Rev. C 88 (2013) 041302(R).
[10] S. Suchyta, et al., Phys. Rev. C 89 (2014) 021301(R).
[11] A. Gade, et al., Phys. Rev. C 81 (2010) 051304(R).
[12] P. Adrich, et al., Phys. Rev. C 77 (2008) 054306.
[13] S.N. Liddick, et al., Phys. Rev. C 84 (2011) 061305(R).
[14] J.N. Daugas, et al., Phys. Rev. C 83 (2011) 054312.
[15] D. Pauwels, et al., Phys. Rev. C 78 (2008) 041307(R).
[16] N. Hoteling, et al., Phys. Rev. C 82 (2010) 044305.
[17] A. Deacon, et al., Phys. Lett. B 622 (2005) 151.
[18] S. Zhu, et al., Phys. Rev. C 74 (2006) 064315.
[19] N. Hoteling, et al., Phys. Rev. C 74 (2006) 064313.
[20] A. Deacon, et al., Phys. Rev. C 76 (2007) 054303.
[21] M.P. Carpenter, et al., Phys. Rev. C 87 (2013) 041305(R).
[22] S. Zhu, et al., Phys. Rev. C 85 (2012) 034336.
[23] National Nuclear Data Center, https://www.nndc.bnl.gov;
K. Abusaleem, B. Singh, Nucl. Data Sheets 112 (2011) 133.
[24] D. von Ehrenstein, J.P. Schiffer, Phys. Rev. 164 (1967) 1374.
[25] I. Čeliković, et al., Phys. Rev. C 91 (2015) 044311.
[26] C. Wraith, et al., Phys. Lett. B 771 (2017) 385.
[27] S. Paschalis, et al., Nucl. Instrum. Methods Phys. Res., Sect. A 709 (2013) 44.
[28] C.Y. Wu, et al., Nucl. Instrum. Methods Phys. Res., Sect. A 814 (2016) 6.
[29] I.-Y. Lee, Nucl. Phys. A 520 (1990) 641c.
[30] T. Lauritsen, et al., Nucl. Instrum. Methods Phys. Res., Sect. A 836 (2016) 46.
[31] The AME2012 atomic mass evaluation, M. Wang, et al., Chin. Phys. C 36 (2012) 1603.
[32] GRETINA Software Working Group, http://gswg.lbl.gov/simulation.
[33] S. Bottoni, et al., to be published.
[34] M. Honma, et al., Phys. Rev. C 80 (2009) 064323.
[35] B.A. Brown, private communication.
[36] A. Bohr, B.R. Mottelson, Nuclear Structure, vol. I, Benjamin, Reading, MA, 1975.
[37] N. Shimizu, et al., Prog. Theor. Exp. Phys. 2012 (2012) 01A205.
[38] M. Honma, et al., Eur. Phys. J. A 25 (Suppl.) (2005) 499.
[39] C.J. Chiara, et al., Phys. Rev. C 85 (2012) 024309.
[40] J.J. Sun, et al., Phys. Rev. C 92 (2015) 054302.
[41] A.D. Ayangeakaa, et al., Phys. Lett. B 754 (2016) 254.